Long-Range Antiferromagnetic Ordering in the Novel Magnetically Frustrated Rock Salt Oxide System: $Li_3Mg_2RuO_6$

Shahab Derakhshan,*[,†,‡] John E. Greedan,[†,‡] Tetsuhiro Katsumata,[†,‡,§] and Lachlan M. D. Cranswick[⊥]

Brokhouse Institute for Materials Research and Chemistry Department, McMaster University, 1280 Main Street West, Hamilton, Ontario, Canada L8S 4M1, and Canadian Neutron Beam Centre, National Research Council Canada Building 459, Chalk River Laboratories, Chalk River, Ontario, Canada K0J 1J0

Received April 28, 2008. Revised Manuscript Received June 16, 2008

The new ruthenate, $Li_3Mg_2RuO_6$, was synthesized in polycrystalline form by a solid-state method. The crystal structure of $Li_3Mg_2RuO_6$ was refined from powder neutron diffraction data in the orthorhombic *Fddd* space group in an ordered NaCl structure type with $a = 5.8759$ (2) Å, $b = 8.4206$ (1) Å, and $c = 17.6455$ (5) Å. The Ru^{5+} ($S = 3/2$) sublattice shows a unique topology, which consists of chains of edge-sharing triangles interconnected by corner sharing and thus there exists the potential for geometric magnetic frustration. This is the first time that magnetic behavior of a material with such sublattice has been investigated. The isostructural, nonmagnetic $Li_3Mg_2NbO_6$ was prepared as the lattice match for the heat capacity analysis. The temperature-dependent magnetic susceptibility, heat capacity, and neutron diffraction data reveal that the system undergoes a long-range AFM ordering below 17 K but also provide evidence for short-range spin correlations well above T_N. The magnetic frustration index, $f \approx 109/17 = 6.4$ suggests that the system is geometrically frustrated. Spin dimer analysis of the magnetic exchange interactions supports this characterization. Comparisons are made with other materials containing the Ru^{5+} ion on geometrically frustrated lattices.

Introduction

Antiferromagnetic (AFM) compounds with triangular cationic sublattices have the potential to exhibit geometric magnetic frustration.[1] This feature is illustrated in Figure 1, from which it is clear that these AFM exchange constraints can not be satisfied simultaneously.

Ordered sodium chloride type transition metal oxides, which have been reviewed recently,[2] are very attractive from this point of view. Within this family there are a number of compositions and structures that present triangle-based topologies. ABO_2 materials with $R\bar{3}m$ symmetry have layers of edge-sharing triangles that alternate... ABAB... along the stacking direction. Examples include the $ACrO_2$ materials, A = Li, Na, and K, which show strong two-dimensional magnetic short-range order (SRO) and frustration indices, defined as $f \sim |\theta|/T_N$, which approach 9 for A = Li.[3,4] Systems with quantum spins, $LiNiO_2$[5,6] and $NaTiO_2$[7] with $S = 1/2$ ions on the same lattice, have been extensively studied as candidates for spin-liquid magnetic ground states, but neither appears to be an appropriate model material. Among ABO_2 types with other symmetries, the thermodynamically stable form of $LiMnO_2$ crystallizing in *Pmmn* and comprising puckered layers of Mn^{3+} ions exhibits short-range, two-dimensional magnetic correlations above 271 K, below which the long-range order sets in.[8] However, the metastable form, *t*-$Li_2Mn_2O_4$ with $I4_1/amd$ symmetry and a distorted version of the pyrochlore lattice (a three-dimensional array of corner-sharing tetrahedra) for the Mn^{3+} ions, is extremely frustrated,

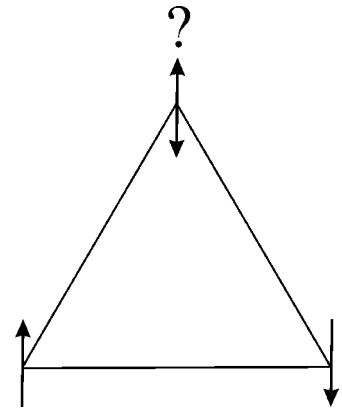

Figure 1. Geometric magnetic frustration in a triangle motif with AFM interactions.

* Corresponding author. E-mail: derakh@mcmaster.ca.
† Brokhouse Institute for Materials Research, McMaster University.
‡ Chemistry Department, McMaster University.
§ Present address: Department of Chemistry, Gakushuin University, 1-5-1 Mejiro, Toshima-ku, Tokyo, Japan 171-8588.
⊥ Chalk River Laboratories.

(1) Greedan, J. E. *J. Mater. Chem.* **2001**, *11*, 37.
(2) Mather, G. C.; Dussarat, C.; Etorneau, J.; West, A. R. *J. Mater. Chem.* **2000**, *10*, 2219.
(3) Delmas, C.; LeFlem, G.; Fouassier, C.; Hagenmuller, P. *J. Phys. Chem. Solids* **1978**, *39*, 55.
(4) Soubeyroux, J. L.; Fruchart, D.; Delmas, C.; LeFlem, G. *J. Magn. Magn. Mater.* **1979**, *14*, 159.
(5) Hirota, K.; Nakazawa, Y.; Ishikawa, M. *J. Phys.: Condens. Mater* **1991**, *3*, 4721.
(6) Reimers, J. N.; Dahn, J. R.; Greedan, J. E.; Stager, C. V.; Liu, G.; Davidson, I.; Vonsachen, U. *J. Solid State Chem.* **1991**, *102*, 542.
(7) Clarke, S. J.; Fowkes, A. J.; Harrison, A.; Ibberson, R. M.; Rossiensky, M. J. *Chem. Mater.* **1998**, *10*, 372.
(8) Greedan, J. E.; Raju, N. P.; Davidson, I. J. *J. Solid State Chem.* **1997**, *28*, 209.

10.1021/cm801161r CCC: $40.75
Published on Web 08/06/2008

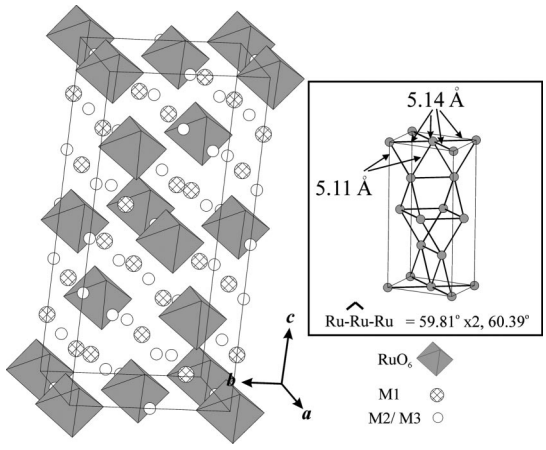

Figure 2. Crystal structure of $Li_3Mg_2RuO_6$. The gray octahedra represent $[RuO_6]^{7-}$; the crossed circles are magnesium-rich (M1) positions and the small empty circles are Li-rich (M2 and M3) positions. The Ru—Ru distances and Ru—Ru—Ru angles are presented in the inset.

showing only two-dimensional spin correlations down to 2 K.[9] Another composition that has received much attention is $A_4B_2O_6$, where B is magnetic and the A sites are diamagnetic. These often form in *C*2/*m* symmetry. Among examples is $Na_3Co_2SbO_6$[10] with a two-dimensional honeycomb lattice of the Co^{2+} magnetic cations, which undergoes AFM long-range order, whereas the isostructural cuprate, $Na_3Cu_2SbO_6$,[11] has a singlet ground state with spin gap behavior and exhibits short-range AFM order below 90 K. The latter system is best described as an AF−AF one-dimensional alternating chain.[12] Finally, the composition A_5BO_6 merits some attention. There are two basic symmetries, *C*2/*m* and *Fddd.* In *C*2/*m*, the magnetic lattice may be described as layers of edge-sharing triangles with some possible connectivity in the third dimension. The $S = 1/2$ compound, Li_4MgReO_6[13] exhibits spin glass behavior below 12 K and no long-range order, whereas the isoelectronic and isostructural Li_5OsO_6 exhibits long-range AFM order at 40 K without any evidence for magnetic frustration.[14] In this report, a *Fddd* material is featured, $Li_3Mg_2RuO_6$, in which Ru^{5+} ($S = 3/2$) is the only magnetic ion. The Ru sublattice in this space group consists of ribbons of edge-sharing triangles along the various [110] directions, which are linked by corners along [001] to form a three-dimensional topology (Figure 2) that should have a high potential for geometric frustration. To the best of our knowledge, this is the first study of a magnetic material with this structure type.

Note that 4d and 5d transition metal ions can be used with great effect in such ordered rock salt structures. Such ions have more extended d orbitals relative to the 3d compounds and they also exhibit large spin−orbit coupling. Moreover, they show a broader range of oxidation states, especially $\geq +5$ rarely seen in 3d elements. The large difference in formal charge between the magnetic cations on one hand and the nonmagnetic alkali and alkali earth cations on the other hand is the driving force toward crystallographic cation ordering in such systems. This allows precise design of the magnetic exchange pathways and interactions.

Because of the wide range of physical properties shown by ruthenates, they have attracted much attention. Although Sr_2RuO_4 is a highly correlated metal and undergoes a superconductivity transition below 1.35 K, both crystallographically different phases of Ca_2RuO_4 are Mott insulators and undergo AFM transitions.[15] Sodium ruthenate, Na_3RuO_4,[16] exhibits three-dimensional magnetic ordering with some degrees of frustration.

In this article, the synthesis and crystal structure along with temperature-dependent magnetic susceptibility and heat capacity data are presented for $Li_3Mg_2RuO_6$. Moreover, to better understand the observed magnetic behavior of the system, we compare the calculated relative magnitudes of the different spin exchange interactions.

Experimental Section

Synthesis. A stoichiometric mixture of Li_2CO_3 (Fisher Scientific, 99.5%; 10% excess), $MgCO_3$ (Baker & Adamson, 99.9% pure), and RuO_2 (Alfa Aesar, 99.95%) was mixed thoroughly and ground. The powder mixture was then pressed into a pellet, placed in an alumina crucible, and heated at 900 °C for 12 h in air and cooled to room temperature over several hours. The pellet was reground and after the addition of an extra 5% Li_2CO_3 was repressed and the same heating schedule repeated.

For $Li_3Mg_2NbO_6$,[17] a stoichiometric mixture of Li_2CO_3 (Fisher Scientific, 99.5%; 10% excess), $MgCO_3$ (Baker & Adamson, 99.9% pure), and Nb_2O_5 (Alfa Aesar, 99.999%) powder was pressed into a pellet, which was placed in an alumina crucible and heated at 950 °C. After 12 h, the furnace was turned off and the sample was cooled over several hours.

Phase Analyses. To examine the phase purity of the brown $Li_3Mg_2RuO_6$ and white $Li_3Mg_2NbO_6$ products, we collected powder X-ray diffraction data, employing a Guinier-Hägg camera with Cu $K\alpha_1$ radiation and Si as an internal standard. The film record was converted to digital data, utilizing a KEJ line scanner.

Crystal Structure and Magnetic Structure Determination Using Neutron Diffraction. Variable-temperature powder neutron diffraction measurements were performed on the C2 diffractometer at the Canadian Neutron Beam Centre at Chalk River, Ontario. The room temperature data were collected using two different wavelengths of 1.3307 and 2.3724 Å.

Low-temperature (K) data sets (4, 6, 8, 10, 12, 14, 16, 17, 18) were collected for investigation of the magnetic structure. For this purpose, the long wavelength, 2.37197 Å in the range $4° \leq 2\theta \leq 84°$ with 0.1° intervals, was utilized.

Physical Properties Measurements. A polycrystalline powder sample of $Li_3Mg_2RuO_6$ was encased in a gelatin capsule and magnetic susceptibility data were collected employing a Quantum Design MPMS SQUID magnetometer. Both zero-field-cooled (ZFC)

(9) Wills, A. S.; Raju, N. P.; Morin, C.; Greedan, J. E. *Chem. Mater.* **1999**, *11*, 1936.
(10) Viciu, L.; Huang, Q.; Morosan, E.; Zandbergen, H. W.; Greenbaum, N. I.; McQueen, T.; Cava, R. J. *J. Solid State Chem.* **2007**, *180*, 1060.
(11) Smirnova, O. A. *J. Solid State Chem.* **2005**, *178*, 1165.
(12) Derakhshan, S.; Cuthbert, H. L.; Greedan, J. E.; Rahman, B.; Saha-Dasgupta, T. *Phys. Rev. B* **2007**, *76*, 104403/1.
(13) Bieringer, M.; Greedan, J. E.; Luke, G. *Phys. Rev. B* **2000**, *62*, 6521.
(14) Derakhshan, S.; Greedan, J. E.; Cranswick, L. M. D. *Phys. Rev. B* **2008**, *77*, 14408/1.
(15) Cao, G.; McCall, S.; Shepard, M.; Crow, J. E. *Phys. Rev. B* **1997**, *56*, R2916.
(16) Regan, K. A.; Huang, Q.; Cava, R. J. *J. Solid State Chem.* **2005**, *178*, 2104.
(17) Mather, G. C.; Smith, R. I.; Skakle, J. M.S.; Fletcher, J. G.; Castellanos, M. A.; Pilar Gutierrez, M.; West, A. R. *J. Mater. Chem.* **1995**, *5*, 1177.

Table 1. Values for the ζ_i Coefficients and Valence Shell Ionization Potentials H_{ii} of the Atomic STOs Employed for the Spin Dimer Calculations for $Li_3Mg_2RuO_6$

atom	orbital	H_{ii} (eV)	ζ_i	C	ζ'_i	C'
O	2s	−32.300	2.688	0.7076	1.675	0.3745
O	2p	−14.8000	3.694	0.3322	1.659	0.7448
Ru	5s	−10.4000	2.091	1		
Ru	5p	−6.870	1.420	1		
Ru	4d	−14.900	4.357	0.5394	2.265	0.5062

and field-cooled (FC) data were obtained over the temperature range of 5−300 K at an applied field of 1000 Oe. The susceptibility data were corrected for core diamagnetism.

Heat capacity data were collected from 4 to 60 K employing the heat capacity probe of the Oxford MagLab system. The powder sample was pressed into a thin pellet and resintered to minimize the grain boundaries. A small piece, ∼0.006 g, was mounted onto a sapphire measurement chip with Apeizon grease. Contributions of grease and sample holder chip to the measured heat capacity were subtracted.

Theoretical Calculations, Spin Dimer Analyses. The relative values of the various spin exchange pathways were estimated by performing the extended Hückel, spin dimer analyses.[18] Because all the exchange pathways in the material involve supersuper exchange (SSE) mechanisms, two RuO_6^{7-} units ($Ru_2O_{12}^{14-}$ dimer) for each pathway were taken into account and the inter site hopping energy, Δe, was estimated using the CAESAR package.[19] For the oxygen s and p and ruthenium d states double-ζ Slater type orbitals were employed whereas single-ζ STO were chosen for ruthenium s and p states. The values of the ζ_i and ζ'_i coefficients and valence shell ionization potentials, H_{ii}, used for the calculations are presented in Table 1. Assuming that $J \cong \langle(\Delta e^2)\rangle/U$ and that U is constant, the relative magnitudes of the various J's can be estimated.

Results and Discussion

Crystal Structure. Rietveld refinements, using the GSAS program,[20,21] on the room-temperature neutron diffraction data sets were performed to investigate the crystal structure. The structural model was initially taken from that proposed by Mather et al.[17] for $Li_3Mg_2NbO_6$. A pseudo-Voigt peak shape profile, which is a convolution of both Gaussian and Lorentzian functions, was chosen and the parameters were refined to obtain the best fit to the experimental data. The overall residual factors of $R_p = 0.0306$, $wR_p = 0.0384$ and $\chi^2 = 3.2$ are rather low, which indicate a good quality refinement (Figure 3.)

$Li_3Mg_2RuO_6$ crystallizes in the orthorhombic *Fddd* space group in an ordered rock salt structure type with lattice dimensions $a = 5.8759$ (2) Å, $b = 8.4206$ (1) Å, and $c = 17.6455$ (5) Å. The structure is composed of edge-shared octahedra with eight formula units per unit cell (Figure 2). There are four independent cationic positions in the unit cell. The oxidation state and size of the Ru^{5+} cations are significantly different from the other cations ($Li^+ = 0.76$ Å, $Mg^{2+} = 0.72$ Å and $Ru^{5+} = 0.565$ Å)[22] and therefore they tend to reside in a separate crystallographic positions. However, the other three cationic sites are mixed occupied by Li and Mg with different fractions, M1 being magnesium-rich, whereas M2 and M3 are lithium-rich sites. When the thermal displacement factors of M2 and M3 sites were refined together, divergence occurred and to stabilize the refinement their U_{iso} values were constrained to a reasonable value, 0.015. This is due to the very small total scattering length in these sites. In fact, the scattering lengths of Li and Mg have opposite signs, $b_{Li} = -1.900$ fm and $b_{Mg} = 5.375$ fm, and the Li:Mg occupancy ratio being close to 4:1 results in a small total negative scattering length, ≈ -0.45 fm. The crystallographic details and the atomic positions are summarized in Tables 2 and 3, respectively.

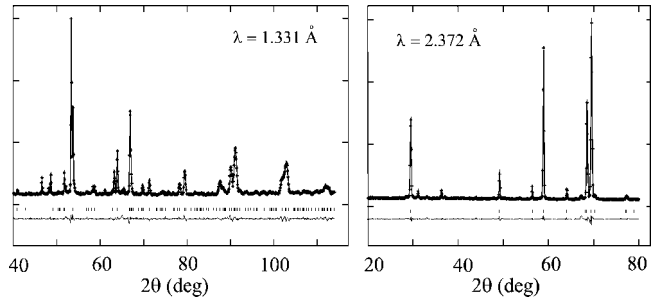

Figure 3. Room-temperature neutron diffraction pattern using long-wavelength (right) and short-wavelength (left) neutrons. The crosses indicate the experimental data, the solid line represents the Rietveld fit, and the thin lines below the pattern the difference. The expected peak positions are located by the vertical tick marks.

Table 2. Some Selected Structural Parameters of $Li_3Mg_2RuO_6$

	a (Å)	b (Å)	c (Å)	Rp	wRp	z
Li_3MgRuO_6	5.8759 (2)	8.4206 (1)	17.6455 (5)	0.0341	0.0472	8

Table 3. Atomic Coordinates, Occupancy Factors, and Equivalent Isotropic Displacement Parameters for $Li_{3.06(1)}Mg_{1.94}RuO_6$

	x	y	Z	Occ. Li/ Mg	U_{iso} (Å^2)
Ru	0.125	0.125	0.125		0.007(1)
M1	0.125	0.125	0.2939(4)	0.33(1)/0.67	0.005(2)
M2	0.125	0.625	0.299(4)	0.78(1)/0.22	0.015
M3	0.125	0.625	0.125	0.82(1)/0.18	0.015
O1	0.125	0.3576(4)	0.125		0.007(1)
O2	0.1114(3)	0.3747(3)	0.2961(2)		0.0069(6)

Magnetic Susceptibilities. For $Li_3Mg_2RuO_6$, the field-cooled susceptibility data overlaid those of zero-field-cooled and therefore only the ZFC data is presented. A peak (Figure 4a) with a maximum near 18 K, is indicative of antiferromagnetic order.

The high-temperature region, from 100−300 K (Figure 4b) fit very well to the Curie−Weiss law, $\chi = C/T - \theta$. The fitting parameters are $C = 1.617(4)$ emu/mol and $\theta = -108.7(5)$ K. The Curie constant corresponds to an effective magnetic moment, μ_{eff}, value of 3.597(6), which is slightly lower than the spin-only effective magnetic moment of the Ru^{5+} ($4d^3$, $S = 1.5$), 3.873 μ_B. This is likely due to the addition of orbital contributions via spin−orbit coupling. According to Hund's third rule for less than half-filled electronic configurations, the orbital

(18) Whangbo, M. H.; Koo, H. J.; Dai, D. J. *J. Solid State Chem.* **2003**, *176*, 417.
(19) Ren, J.; Liang, W.; Whangbo, M. H. Crystal and Electronic Structure Analysis Using CAESAR. http://www.primeC.com (2005).
(20) Larson A. C., Von Dreele R. B. *General Structure Analysis System (GSAS)*; Los Alamos National Laboratory Report LAUR 86-748; Los Alamos National Laboratory: Los Alamos, NM, 2000.
(21) Toby, B. H. *J. Appl. Crystallogr.* **2001**, *34*, 210.
(22) Shannon, R. D. *Acta Crystallogr., Sect. A* **1976**, *32*, 751.

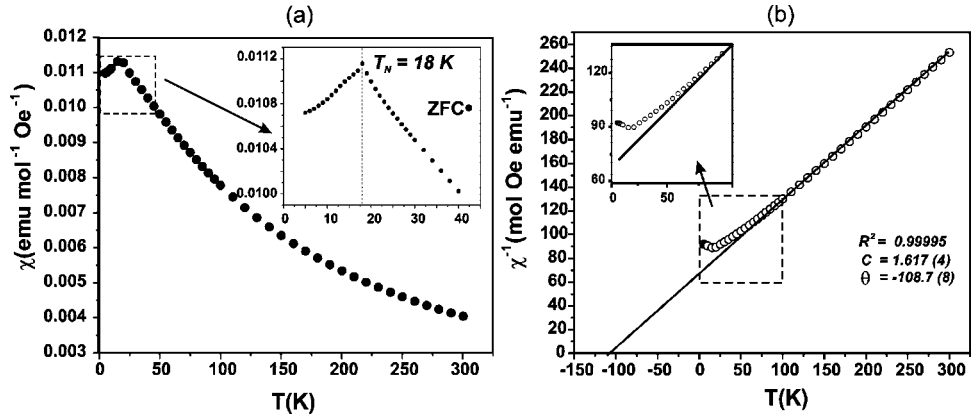

Figure 4. (a) Temperature-dependent, zero-field-cooled magnetic susceptibility data for $Li_3Mg_2RuO_6$. The insets clarify the transition temperature. (b) Curie−Weiss fit in the high-temperature, paramagnetic region for $Li_3Mg_2RuO_6$. The open circles denote the ZFC data points and the solid line is the fit. The insets show the deviation from Curie−Weiss behavior, which sets in well above T_N.

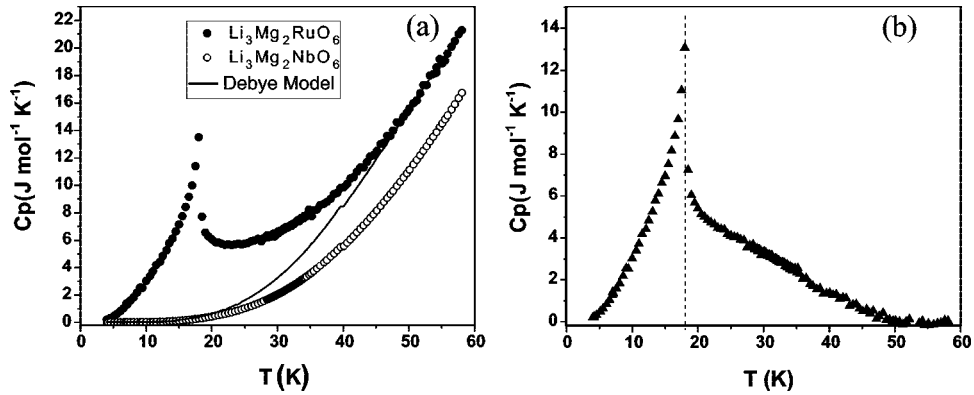

Figure 5. (a) Temperature-dependent heat capacity data for $Li_3Mg_2RuO_6$ (filled circles) and the lattice match $Li_3Mg_2NbO_6$ (open circles). The solid line indicates the lattice contribution based on the Debye model. (b) The difference plot represents the magnetic contribution to the heat capacity.

component substracts from the spin part, resulting in a magnetic moment with a lower value than that of the spin-only case.

On the basis of the mean field theory, the relationship between the Weiss temperature and the various exchange constants, J_m, is given by[23]

$$\theta = \frac{2S(S+1)}{3k_B}\sum_{m=1}^{N} z_m J_m \qquad (1)$$

where θ is the Weiss constant, J_m is the exchange interaction between mth neighbors, z_m is the number of mth nearest neighbors of a given atom, and N is the number of sets of neighbors for which $J_m \neq 0$. The so-called frustration index, $f \approx |\theta|/T_N$, can be applied to determine the extent of the magnetic frustration in this material.[24] If $f > 5$, the system is considered frustrated and therefore $Li_3Mg_2RuO_6$ with $f \approx 6.4$ is a frustrated system, by this criterion.

Heat Capacity Data. Heat capacity data for $Li_3Mg_2RuO_6$ are presented in Figure 5a as filled black circles. The lambda anomaly peaking at 18 K is further evidence for long-range AF magnetic order at this temperature. In an attempt to estimate the lattice contribution to the heat capacity, comparable data were collected for isostructural $Li_3Mg_2NbO_6$ (open circles in Figure 5a).This material was chosen as Nb^{5+} is diamagnetic and similar in mass to Ru^{5+}. However, as is clear from Figure 5a, the two data sets do not converge within the temperature range investigated. Thus, a direct subtraction was not possible so a different approach was adopted.[25] According to the Debye model, the heat capacity can be expressed as in eq 2

$$\frac{C_P}{3R} = \frac{3}{x^3}\int_0^x \frac{x^4 e^x \, dx}{(e^x - 1)^2} \qquad (2)$$

where R is the gas constant and $x = \theta_D/T$ with θ_D being the Debye temperature. $C_P/3R$ values are tabulated for various x. [26] If it is assumed that in the high temperature regime the magnetic contribution is small and the lattice term is dominant for both materials, the data for $Li_3Mg_2NbO_6$ can be scaled using a suitable procedure. In this case, θ_D values were calculated from eq 2 within the range 49 to 59 K, and it was discovered that this quantity is temperature dependent for both materials. Thus, a temperature-dependent scaling factor was determined and applied to the $Li_3Mg_2NbO_6$ data at all temperatures to obtain the lattice match approximation shown as the solid line in Figure 5a. Subtracting this from the data for $Li_3Mg_2RuO_6$ gives an estimate of the magnetic contribution, Figure 5b.

(23) Smart, J. S. *Effective Field Theory of Magnetism*; W. B. Saunders Company: Philadelphia, 1966.
(24) Schiffer, P.; Ramirez, A. P. *Comments Condens. Matter Phys.* **1996**, *10*, 21.
(25) Wiebe, C. R.; Greedan, J. E.; Luke, G.; Gardner, J. S. *Phys. Rev. B* **2002**, *65*, 144413.
(26) Gopal, E. S. R.; *Specific Heats at Low Temperatures*; Plenum Press, New York, 1966.

The total entropy loss can be calculated using equation 3 and the data of Figure 6.

$$\Delta S_{\text{exp}} = \int_0^T \left(\frac{C_{\text{P}}}{T}\right) \mathrm{d}T \tag{3}$$

The full entropy loss is determined as $\Delta S = 8.00$ J/(mol K). This can be compared to the theoretical entropy loss given by the Boltzmann equation, eq 4

$$\Delta S_{\text{theor}} = R \ln \omega \tag{4}$$

where $\omega = 2S + 1 = 4$ for $S = 3/2$ and $\Delta S_{\text{theor}} = 11.53$ J/(mol K). Thus, the observed ΔS is 69% of ΔS_{theor}. This suggests some shortcomings in the procedure used to estimate the lattice contribution but this is the best that can be obtained given the limitations of the data. The entropy loss associated with the phase transition is obtained by integration of Figure 6 below T_{N} and the result is 4.69 J/(mol K), which is only 59% of the total loss.

Given the discussion above, this is likely an overestimation. These results are further evidence for the importance of short-range magnetic correlations in this material. This observation is in agreement with the susceptibility data, which show a deviation from the Curie−Weiss law below 75 K (inset in Figure 4c).

Computational Methods: The Tight Binding, Spin Dimer Model. Figure 7 shows the Ru sublattice, which can be described as orthogonal chains of edge-shared triangles that are connected by corner sharing. In principle, this topology presents the condition for geometric frustration but it remains to determine the signs and relative magnitudes of the various exchange pathways in this material. These are all of the supersuper exchange (SSE) type, Ru−O−Li(Mg)−O−Ru, and the four most important of these out to a Ru−Ru distance of 6.85 Å are shown in Table 4.

For a d^3 system in an octahedral crystal field, d_{xy}, d_{xz}, and d_{yz} orbitals are degenerate and it is a valid approximation that the probability that they contribute to the exchange interactions is equal, and we have

$$\langle (\Delta e)^2 \rangle \approx \frac{1}{N^2} \sum_{\mu=1}^{N} (\Delta e_{\mu\mu})^2 \tag{5}$$

In these systems, there are three states that are involved, and therefore, eq 5 can be re arranged as

$$\langle (\Delta e)^2 \rangle \approx \frac{1}{9} [(\Delta e_{11})^2 + (\Delta e_{22})^2 + (\Delta e_{33})^2] \tag{6}$$

and finally the spin exchange interactions will be given by

$$J \cong \frac{\langle (\Delta e)^2 \rangle}{U} \tag{7}$$

The corresponding relative exchange interactions were calculated and the results are presented in Table 5.

To examine the consistency of the calculations, different values of $(1-x) \times \zeta'_{\text{i}}$ with $x = 0$, 0.05, and 0.1 for oxygen 2p atomic orbitals were employed and similar relative values were obtained. ζ'_{i} describes the diffuse STO and, by providing an orbital tail, enhances the overlap between oxygen atoms within the SSE pathways.[27]

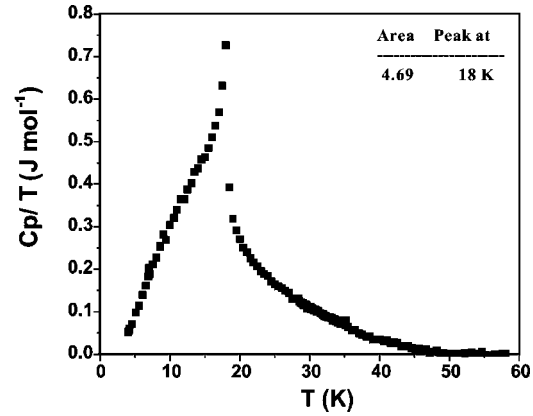

Figure 6. C_{P}/T as a function of temperature. The area under the peak represents magnetic entropy for the transition in $Li_3Mg_2RuO_6$.

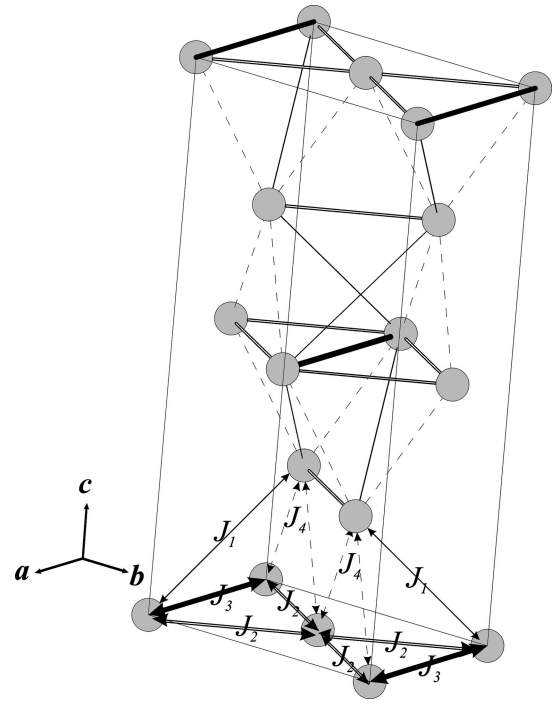

Figure 7. Schematic representation of different possible Ru−Ru interaction pathways in the unit cell. J_1 is shown by the thin lines, J_2 and J_3 are represented by the gray and black thick lines, respectively, and J_4 is indicated by the dashed lines.

From Table 5, it is clear that J_3 and J_2 are the dominant interactions, being much greater than J_1, although this is the shortest Ru−Ru distance. Note that J_2 and J_3 form an array of edge-sharing triangles in the *ab* plane, which also represents geometric frustration but in two dimensions rather than three as the interplanar pathways, J_1 and J_4, are weaker by a factor of 10^2.

Low temperature neutron diffraction data were collected to probe the magnetic structure as shown in Figure 8. There are at least five additional peaks in the low temperature data which correspond to the magnetic structure. Subtracting the 18K data from those of the 4 K their positions are identified as shown in Figure 8. They clearly disappear by 18 K, Figure

(27) Koo, H.-J.; Lee, K.-S.; Whangbo, M.-H. *Inorg. Chem.* **2006**, *45*, 10743.

Table 4. Relevant Distances to the Four Identified Exchange Pathways, J_1, J_2, J_3,and J_4

J_1 (Å)	J_2 (Å)	J_3 (Å)	J_4 (Å)
5.105	5.877	5.135	6.583

Table 5. $(\Delta e)^2$ for the Various Exchange Pathways in $Li_3Mg_2RuO_6$ Calculated on the Spin Dimer Model

pathway	$Li_3Mg_2RuO_6$ $(\Delta e)^2$ $(meV)^2$	rel.
J_1	158	0.04
J_2	**1149**	**0.32**
J_3	**3554**	**1**
J_4	58	0.02

9, consistent with both the susceptibility and specific heat data. The two major peaks were indexed using a LeBail approach which required a magnetic cell of dimensions $2a \times 2b \times 3c$ relative to the chemical cell, giving indices (1/2 1 1/3) and (1/2 1/2 2). Thus, the magnetic cell is 12 × the volume of the chemical cell and involves $8 \times 12 = 96$ Ru spins. Attempts to solve the magnetic structure are ongoing but this is clearly a difficult and highly underdetermined problem. While the details of the magnetic structure are not known in detail, the large dimensions of the magnetic unit cell are consistent with a high level of frustration in three dimensions, in spite of the conclusion from the spin dimer analysis which suggests a more two-dimensional picture. As well, the symmetric shape of the magnetic diffuse scattering at 18K, seen clearly in Figure 9, is not consistent with short-range 2D magnetic correlations for which the highly asymmetric "Warren" line shape is expected and which has been observed in the related material $Li_2Mn_2O_4$.[9]

Conclusion

The novel ruthenate $Li_3Mg_2RuO_6$ was synthesized and its crystal structure was investigated, using room temperature powder neutron diffraction data. This compound crystallizes in an ordered rock salt structure type in *Fddd* space group with the lattice parameters of $a = 5.8759$ (2) Å, $b = 8.4206$ (1) Å and $c = 17.6455$ (5) Å. Ru^{5+} reside in a distinct crystallographic position whereas the other three cationic positions exhibit Li^+/ Mg^{2+} mixing. This is the first known investigation of the magnetic properties of a material with this specific magnetic sublattice topology. The temperature-dependent magnetic susceptibility data shows $\theta = -109$ K and AFM long-range order below 17K and frustration index $f \approx 6.4$. Both susceptibility and heat capacity data, when entropy removal is taken into account, show evidence for short-range AFM correlations well above T_c. Spin dimer analysis was performed and the results were consistent with a frustrated triangular lattice model with dominant *ab* plane exchange and weaker interactions in the *c*-direction. Low temperature neutron diffraction data indicate $T_N = 17$ K but with a magnetic unit cell which is 12 times the volume of the chemical cell, involving 96 Ru spins which has not yet been solved. The diffuse magnetic scattering above T_c is symmetric and clearly not of the Warren type. All of the above observations indicate a high degree of magnetic frustration in three dimensions. That long-range magnetic order does occur, eventually, is in line with the known behavior of other materials with the same ion, Ru^{5+}, $S = 3/2$, on geometrically frustrated lattices. Examples are found

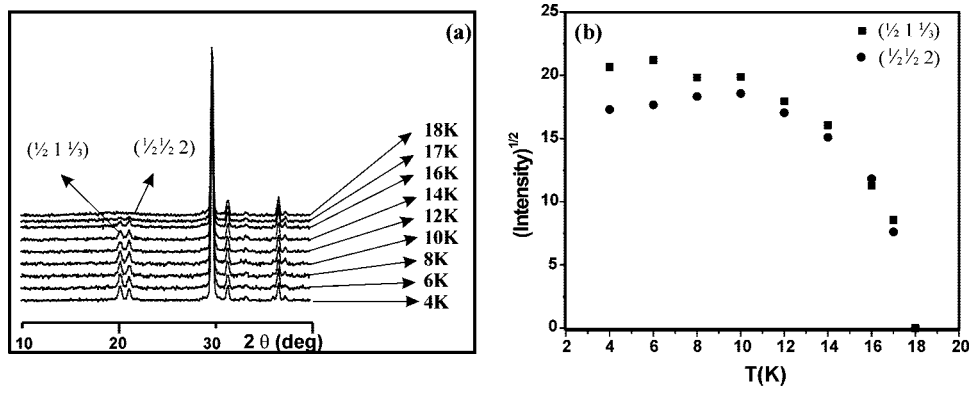

Figure 8. (a) Low-temperature powder neutron diffraction data. (b) Integrated area for magnetic peaks as a function of the temperature.

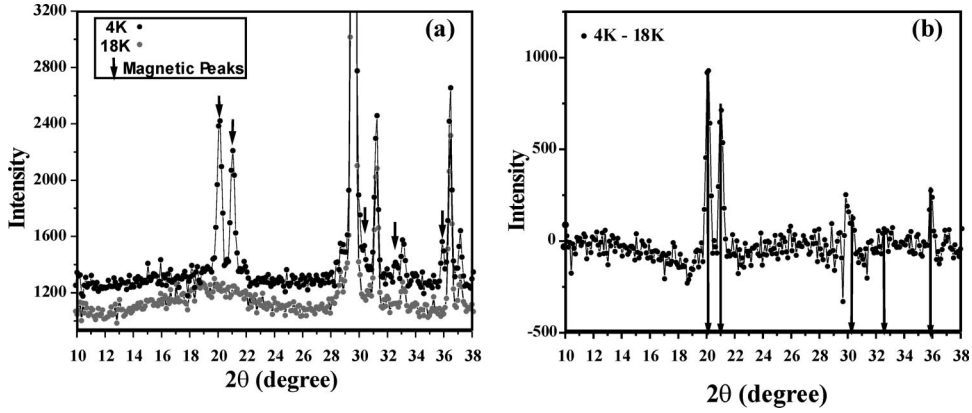

Figure 9. (a) Comparison between diffraction patterns at 4 and 18 K. (b) Magnetic peaks obtained by subtracting the 18 K data from the 4 K data.

among the B-site ordered double perovskites, Ba_2MRuO_6 (M = Y,Lu) and La_2LiRuO_6. Here the B-site crystallographic ordering results in a Ru^{5+} sublattice of fcc topology—a three-dimensional lattice of edge-sharing tetrahedra—one of the canonical geometrically frustrated lattices. The Ba phases order below 35 K and the La phase below 30 K with frustration indices of ~18 (M = Lu) and 9, respectively.[28,29] It would be of considerable interest to study systems with "quantum" spins, $S = 1$ or 1/2 on the new magnetic lattice described here. Initial attempts in this direction have been unsuccessful but efforts are on going.

Acknowledgment. We thank Paul Dube for his assistance in collecting magnetic susceptibility and heat capacity data. We appreciate fruitful discussions with Craig Bridges and Andrew Wills. J.E.G. acknowledges the Natural Sciences and Engineering Research Council of Canada for financial support of this work.

Supporting Information Available: One neutron crystallographic file (CIF). This material is available free of charge via the Internet at http://pubs.acs.org.

CM801161R

(28) Battle, P. D.; Jones, C. W. *J. Solid State Chem.* **1989**, *78*, 108.

(29) Battle, P. D.; Grey, C. P.; Hervieu, M.; Martin, C.; Moore, C. A.; Paik, Y. *J. Solid State Chem.* **2003**, *175*, 20.